Ciliary motion modeling, and dynamic multicilia interactions

Shay Gueron and Nadav Liron
Department of Mathematics, Technion-Israel Institute of Technology, Haifa 32000, Israel

ABSTRACT This paper presents a rigorous and accurate modeling tool for ciliary motion. The hydrodynamics analysis, originally suggested by Lighthill (1975), has been modified to remove computational problems. This approach is incorporated into a moment-balance model of ciliary motion in place of the previously used hydrodynamic analyses, known as Resistive Force Theory. The method is also developed to include the effect of a plane surface at the base of the cilium, and the effect of the flow fields produced by neighboring cilia. These extensions were not possible with previous work using the Resistive Force Theory hydrodynamics. Performing reliable simulations of a single cilium as well as modeling multicilia interactions is now possible. The result is a general method which could now be used for detailed modeling of the mechanisms for generating ciliary beat patterns and patterns of metachronal interactions in arrays of cilia. A computer animation technique was designed and applied to display the results.

1. INTRODUCTION

Ciliary and flagellar propulsion have attracted a great deal of research effort both experimentally and theoretically. The use of mathematical modeling to simulate the internal mechanism of cilia ("internal" models) has been extensively developed (Sleigh, 1962; Brokaw, 1970, 1972*a*, 1972*b*, 1975, 1976; Rikmenspoel, 1973, 1976, 1982; Brokaw and Rintala, 1975, 1977; Hines and Blum, 1978, 1979*a*, 1979*b*, and others). So far it has only been possible to simulate the motion of a single cilium (or flagellum), as an initial value problem. Multicilia configurations have not been modeled this way. Instead, "external" models, where metachronal patterns are presumed, were used to deal with this phenomenon (Blake, 1972; Liron and Mochon, 1976; Liron, 1978, 1984). These models did not produce metachronism as the result of a time dependent process, but assumed its existence.

The motion of cilia and flagella which takes place in a highly viscous and incompressible surrounding fluid, is governed by the Stokes equations with no-slip boundary conditions on their surfaces (i.e., the velocity of the fluid on the surface matches the velocity of the surface), and vanishing fluid disturbance (i.e., zero fluid velocity) at infinity. The Stokes equations neglect the effect of inertial forces. This assumption is reasonable for cilia (and flagella) because of their small dimensions, typical velocities, and the typical viscosity of the fluid they are found in (water) (see e.g., Brennen and Winet, 1977). It follows that one may apply equations of mechanical equilibrium (balance of forces and moments) to the problem. Since the Stokes equations are linear, it is possible to construct a solution, satisfying part of the (no-slip) boundary conditions, by superposing fundamental (singular) solutions. The fact that cilia and flagella are slender suggests certain asymptotic approximations, used to relate the local drag forces (exerted on the cilium by the surrounding fluid) to the local velocity. Such an approach was pioneered by Gray and Hancock (1955) (G-H henceforth), and was used in all of the above "internal" models. In this approach the (tangential, normal, and binormal) components of the drag force are assumed to be proportional to the components of the velocity, with different proportionality constants for each one. The reason for the extensive use of the G-H approximation, which is a local relation, is that it is relatively easy to implement. The G-H approximation has severe limitations, however, and has been subjected to criticism (Lighthill, 1975, 1976; Childress, 1981). It had been originally stated in connection with an infinite cylinder moving in an infinite and motionless medium. In this case the local drag force is indeed proportional to the local velocity (with appropriate constants of proportionality for each component, called resistance coefficients). This relation was applied to flagella and cilia, using their slenderness property (each segment along a cilium was treated as a part of a long cylinder moving in the infinite medium). Small curvature (compared with the length of the cilium) is therefore implicitly assumed. Since this is usually not the case, applying the G-H approach to cilia and flagella already violates its fundamental assumption. In the G-H approach the cilium is considered to be moving in a motionless medium, except for the flows created by the movements of its own segments. The effect of these flows is supposedly taken into account by the "effective" resistance coefficients. These constants of proportionality are those applicable for a cylinder (which should be long with respect to the radius of the cilium, but short with respect to the cilium's length) moving in a viscous fluid. This somewhat ad-hoc argumentation is not amenable to error estimates. Also, the G-H approximation cannot consider the effect of the hydrodynamic interaction of cell bodies (to which flagella are attached) or flat surfaces (to which cilia are anchored). Therefore, it is limited only to the cases of flagella which are free at both ends. It also lacks even heuristic justification in rela-

Shay Gueron is currently at the Center for Applied Mathematics, 305 Sage Hall, Cornell University, Ithaca, NY 14853.

tively large portions adjacent to these ends (e.g., Brokaw, 1970). Moreover, when numerically applied to simulate ciliary (flagellar) beats, it did not match the exact (or experimental) solutions. To overcome these drawbacks, the use of altered drag coefficients has been attempted (Lighthill, 1975; Brennen and Winet, 1977; Johnson and Brokaw, 1979). These attempts are known as 'Resistive Force Theories' (RFT henceforth). Some authors (Brokaw, 1970) determined experimentally (so-called) suitable coefficients for specific cases (isolated flagellum in water), in order to match the results to known data. Johnson and Brokaw (1979) compared the results of the G-H approximation to results which are obtained by more accurate methods. They reported that an empirical 35% increase in the drag coefficient, "corrected" the G-H approximation for a two sided end-free flagellum. However, they could not correct the G-H approach to match accurate solutions, when a cell body was attached to the flagellum. Even if one could somehow obtain coefficients accurately modelling the motion of a single cilium, there is no justification to cases where it moves in external flows. In these cases the effective resistance coefficients are expected to depend on the external flow. There is no reason to believe that these coefficients would remain constant along the cilium (at all times) under such conditions. Thus, RFT could not be applied to multicilia configurations.

A more consistent method to relate drag forces and velocity, for an infinite flagellum, has been suggested by Lighthill (Lighthill, 1976) and rigorously proved by Childress (Childress, 1981) (although he obtained a larger error estimate than what Lighthill had predicted). Lighthill's formula is a vectorial integral equation for the drag forces. Unfortunately, this equation is an integral equation of the first kind (with respect to its tangential component) and is therefore ill posed. In addition, its integrand is singular and the integration interval contains points that are very close to the singularity. This introduces severe problems in any attempt at a numerical solution.

Other hydrodynamic analyses, generally referred to as Slender Body Theory (SBT), have been further developed and refined by numerous authors. They were applied to various problems involving flagellar motion, offering different methods to relate between the drag forces and the velocities. Johnson and Brokaw (1979) used SBT and applied it to flagellar simulations as a cross reference for results obtained by RFT. It was reported there that the computational effort added by using SBT outweighed the gained additional accuracy in the case of a single isolated flagellum with no cell body attached to it. This conclusion changed when a cell body was added. Dresdner, Katz, and Berger (1980), and Higdon (1979*a*) also used variants of SBT for large amplitude planar motions of a flagella with and without spherical cell bodies. Other papers dealt with helical motions of flagella with and without cell bodies (e.g., Higdon [1979*b*], Phan-Thien, Tran-Cong, and Ramia [1987], Myerscough and Swan [1989], Ramia [1991]). Higdon (1979*c*) treated a flagellum standing on a stalk and accounted for the effect of a (far) plane from which the stalk emerges.

Our purpose is to present a method which overcomes the difficulties associated with Lighthill's method, while being applicable for multicilia configurations. After introducing several useful notations in Section 2, we present, in Section 3, a variation on Lighthill's equation. This variation generates a well posed integral equation of the second kind for all components, keeping the integration interval away from the singularity. The equation is similar to the G-H approximation (with different resistance coefficients) together with correcting terms. The correcting terms result from a similar analysis to that which provided the basis for Lighthill's theorem.

Our equation depends on an arbitrary parameter. In Section 3 we prove and also demonstrate (in Section 7) the fact that this parameter may be chosen within a wide range with no significant effect on the results, thus justifying our approach. A similar approach, for two-dimensional motion of a flagellum, with or without a spherical head attached to it, was developed by Dresdner, Katz, and Berger (1980).

Equipped with this applicable drag-velocity equation we combine it (after some necessary modifications) with the geometric equations and the two-dimensional equilibrium equations (suggested by Hines and Blum [1978], H.-B. henceforth) to model ciliary beats. This procedure is described in Section 4. The equation of the internal mechanism is inserted in a "modular" manner (i.e., it can be changed so as to fit other desired models). Since we were not interested in any particular mechanism we constructed one of our own as detailed in Section 5. It produced beat patterns similar to beats observed in biological experiments. Other mechanisms can also be tested using our method. The precise choice of the parameters used in our simulations, and the numerical methods are summarized in Section 6.

After investigating one cilium we moved on to multicilia configurations, treating them as dynamic development problems. This is not possible using the G-H approximation, and has not been performed using Lighthill's approach. Our investigation enables to approximate the maximal spacing between cilia where they still influence one another, and to examine the changes of the beat patterns in the presence of neighboring cilia. The effect of increasing the surrounding fluid viscosity, on an array of beating cilia, has also been analyzed. These results are reported in Section 7.

It is well known that when adjacent cilia beat near each other, metachronism is formed. Metachronism is a state where a phase lag between the cilia exists, and a travelling wave is formed by their moving tips. Our approach, being suitable for modelling multicilia configurations, presents a general method for the investigation of

metachronism, as mentioned in the Discussion (Section 8) that concludes the paper.

2. NOTATIONS

In order to make the paper shorter and clearer we adopt several notations and conventions that will be used henceforth.

The cilium is modelled as an inextensible (i.e., maintaining a constant length at all times) cylindrical filament of length L. The center line of the filament is a curve, parameterized by its arclength parameter s ($0 \leq s \leq L$: $s = 0$ at the "anchor" where the cilium is attached to a surface, and $s = L$ at the [free] distal end).

We define the three axes $\mathbf{x}_1\ \mathbf{x}_2\ \mathbf{x}_3$ as in Fig. 1 *a* and set $\mathbf{x}_3 = 0$ at the cilium's anchor. Whenever dealing with a single cilium, its anchor is located at the origin. The location of the anchors for multicilia configurations will be specified in the examples.

All locations and forces in our problem depend both on the time t and on s. We omit writing this dependence explicitly, whenever it is obvious from the context.

At each point on the cilium (curve) we refer to two sets of coordinates. The first one represents the (global) location ($\mathbf{x}_1$, $\mathbf{x}_2$, $\mathbf{x}_3$) (with respect to some fixed origin) and the other is the local Frenet trihedron ($\mathbf{T}(s, t)$, $\mathbf{N}(s, t)$, $\mathbf{B}(s, t)$) (tangential, normal, and binormal unit vectors, respectively). Whenever the problem is planar the system reduces to ($\mathbf{T}$, $\mathbf{N}$) and ($\mathbf{x}$, $\mathbf{y}$) (Fig. 1 *b*).

The subscripts T, N, B denote the tangential, normal, and binormal components of vectors, respectively, and the subscripts s and t denote partial differentiation with respect to s and to the time, t, respectively.

We define $\epsilon = a/L$, the ratio of the radius of the cilium a to its length L, to be the slenderness parameter. It is assumed that $\epsilon \ll 1$.

The geometrical equations for the two-dimensional model have already been formed by H.-B. Consequently, we adapt their notations as follows: $\alpha(s, t)$ ($=\alpha$) is the angle between the curve's tangent and the x_1 (or x) axis, see Fig. 1 *b*. The curvature is denoted by k and satisfies

$$k = \alpha_s. \tag{2.1}$$

We use $\mathbf{F}(s, t)$ ($=\mathbf{F}$) to denote the shear force developed by the internal mechanism of the cilium and $\mathbf{M}(s, t)$ ($=\mathbf{M}$) for the (binormal) bending moment it produces. $\boldsymbol{\phi}(s, t)$ ($=\boldsymbol{\phi}$) is the force per unit of length (i.e., drag force) exerted on the cilium by the surrounding fluid in which the cilia beat. $\mathbf{V}(s, t)$ ($=\mathbf{V}$) is the velocity of the cross-section s, and μ is the viscosity of the surrounding fluid.

3. RELATION BETWEEN THE DRAG FORCES AND THE LOCAL VELOCITY

As already outlined in the Introduction, in order to construct a reasonable model, the presence of a (flat) sub-

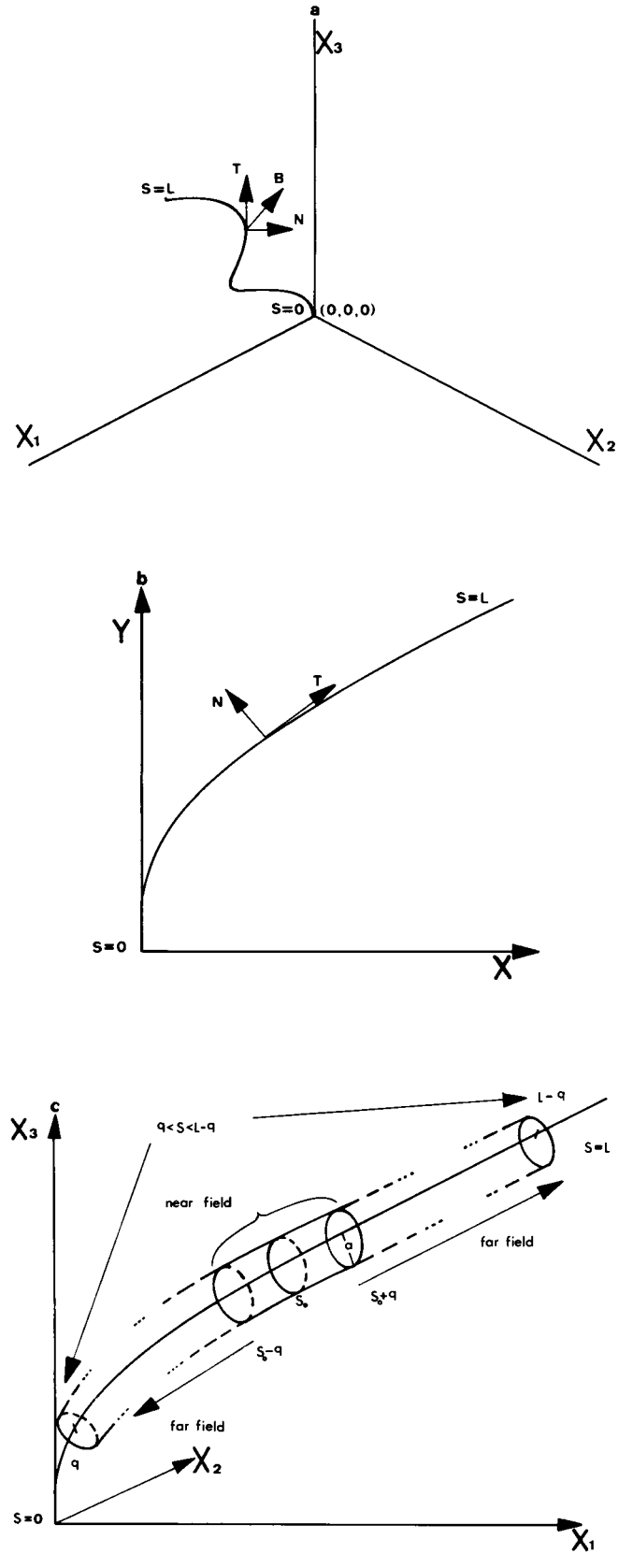

FIGURE 1 (*a*) Local and global coordinate systems, three-dimensional. (*b*) Local and global coordinate systems, two-dimensional. (*c*) Near and far field of a location s_0, on a cilium (see Eq. 3.3 (not to scale)).

strate (from which the cilia emerge) must be accounted for. Moreover, possible external flows must also be introduced, to enable the modeling of hydrodynamic interaction between cilia. All early simulations, (that used RFT) of ciliary (and flagellar) motion were limited to the modeling of a single cilium (flagellum) free at both ends (i.e., without a cell body for a flagellum of a flat substrate for a cilium), moving in motionless fluid. Whenever a cell body was modeled too, the authors resorted to more sophisticated analyses than RFT, namely SBT (e.g., Brokaw and Johnson, 1979; Higdon, 1979*a*, 1979*b*, 1979*c*; Dresdner, Katz, and Berger, 1980; Phan-Thien, Tran-Cong, and Ramia, 1987; Myerscough and Ramia, 1989; Ramia, 1991). Higdon (1979*c*) also treated the influence of a flat wall in the case of a flagellum with a spherical head, standing on an erect stalk. One should note that in his paper the distance from the wall is kept $O(L)$ (which is not the case for cilia). However, "internal models" considering cilia attached to a pane surface have not been dealt with. The RFT models involved the use of the G-H approximation namely:

$$\phi_T = -C_T V_T, \quad \phi_N = -C_N V_N, \quad \phi_B = -C_B V_B \quad (3.1)$$

(the constants C_T, C_N, C_B are the resistance coefficients).

Correcting the resistance coefficients (RFT) works in some restricted cases, but in general no RFT can be applied to the modeling of cilia attached to a flat surface, nor can they be extended to account for external flows (e.g., multicilia configurations).

Using the linearity of the Stokes equations, which govern the motion of cilia and flagella, and using their slenderness property, Lighthill (1976) suggested a more accurate approach to relate drag forces and velocities. He wrote down the following expression for the velocity (in terms of the drag force), which becomes an integral equation if the drag force is to be calculated (which is usually the case).

$$\mathbf{V}(s_0, t) = (-\tfrac{1}{4}\pi\mu)\phi_N(s_0, t)\mathbf{N} - (\tfrac{1}{4}\pi\mu)\phi_B(s_0, t)\mathbf{B} + \int_{|s-s_0|>a\sqrt{e}/2} \mathbf{U}_s(\mathbf{r}(s, t), \mathbf{r}(s_0, t), -\boldsymbol{\phi}(s, t))\, ds. \quad (3.2)$$

The integrand $\mathbf{U}_s(\mathbf{r}(s, t), \mathbf{r}(s_0, t), -\boldsymbol{\phi}(s, t))$ in (Eq. 3.2) is the velocity (which is a singular fundamental solution of the Stokes equations, see Appendix) induced by a Stokeslet of strength $\boldsymbol{\phi}(s, t)$ located at $\mathbf{r}(s, t)$, with intensity $-\boldsymbol{\phi}(s, t)$, located at $\mathbf{r}(s_0, t)$ (see the theorem below for notations). Here, the pronumeral e is the famous irrational number $e \approx 2.718$ (i.e., $\frac{1}{2}a\sqrt{e} \approx 0.82a$).

Lighthill's theorem has been rigorously proved by Childress (1981), although his estimate for the error ($O(\sqrt{\epsilon})$) was larger than what Lighthill had predicted ($O(\epsilon)$). Nevertheless, no simulations using Lighthill's method were reported. The only terms that are explicit (i.e., not in the integral) in Lighthill's equation are normal and binormal components. The tangential component of this equation is therefore an integral equation of the first kind, which is known to be more difficult to solve than integral equations of the second kind (and generally form ill posed problems). Moreover, the minimal distance from the singularity (the Stokeslet is singular at $\mathbf{r}(s, t) = \mathbf{r}(s_0, t)$), along the interval of integration, is as small as $0.82a$. Hence, it is clear that any attempt at a numerical solution of the problem will potentially encounter severe difficulties.

In what follows we present an appropriate way to overcome the above limitations. A modification of Lighthill's equation divides it into two parts and makes it an integral equation of the second kind. The first part consists of local contributions, exactly as in the G-H approach (but with different coefficients). The second part contains the contributions of the distant segments of the same cilium, the effect of the flat substrate from which the cilia emerge, and the effect of possible external flows. The integration interval is kept far from the singularity. The equation seems to depend on an arbitrary constant q, but the solution itself will be shown to be independent of it. Dresdner, Katz and Berger (1980) used a similar approach for the propulsion of a uniflagellar microorganism (sphere with a flagellum attached to it), and gave a heuristic argument why this should be true. Consequently, they do not have an error estimate. Our theorem puts their approach on a sound footing, shows the proper range for q, gives an error estimate for the entire SBT approximation, and consistently includes external flows, wall effects, and is true for general three-dimensional motions.

We now state our theorem.

Theorem

Let $\mathbf{r}(s, t)$ be the location of the center line of a cilium ($0 \le s \le L$) of radius a, attached to a flat surface at $x_3 = 0$. We use the following notations for any two location vectors $\mathbf{r}$ and $\mathbf{r}_0$ and intensity vector $\boldsymbol{\phi}$ (see Appendix for explicit expressions):

$\mathbf{U}_s(\mathbf{r}, \mathbf{r}_0, \boldsymbol{\phi})$ = the velocity, induced at $\mathbf{r}$, by a Stokeslet with intensity $\boldsymbol{\phi}$, located at $\mathbf{r}_0$ (in infinite medium).

$\mathbf{U}_{si}(\mathbf{r}, \mathbf{r}_0, \boldsymbol{\phi})$ = the velocity, induced at $\mathbf{r}$, by a Stokeslet located at $\mathbf{r}_0$, with intensity $\boldsymbol{\phi}$, and by its image system (i.e., this is a basic solution satisfying no-slip conditions at $x_3 = 0$).

$\mathbf{U}_d(\mathbf{r}, \mathbf{r}_0, \boldsymbol{\phi})$ = the velocity, induced at $\mathbf{r}$, by a Doublet with intensity $\boldsymbol{\phi}$, located at $\mathbf{r}_0$ (in infinite medium).

$\mathbf{U}_{di}(\mathbf{r}, \mathbf{r}_0, \boldsymbol{\phi})$ = the velocity, induced at $\mathbf{r}$, by a Doublet, located at $\mathbf{r}_0$, with intensity $\boldsymbol{\phi}$, and by its image system (i.e., this is a basic solution satisfying no-slip conditions at $x_3 = 0$).

$\mathbf{V}_{si}(\mathbf{r}, \mathbf{r}_0, \boldsymbol{\phi}) = \mathbf{U}_{si}(\mathbf{r}, \mathbf{r}_0, \boldsymbol{\phi}) - \mathbf{U}_s(\mathbf{r}, \mathbf{r}_0, \boldsymbol{\phi})$ (i.e., the velocity induced by the image system of a Stokeslet alone).

$\mathbf{V}_{di}(\mathbf{r}, \mathbf{r}_0, \boldsymbol{\phi}) = \mathbf{U}_{di}(\mathbf{r}, \mathbf{r}_0, \boldsymbol{\phi}) - \mathbf{U}_d(\mathbf{r}, \mathbf{r}_0, \boldsymbol{\phi})$ (like $\mathbf{V}_{si}$ but relating to a Doublet)

(no-slip conditions imply here vanishing velocities on the plane $x_3 = 0$).

Let $q = O(a/\sqrt{\epsilon})$ and $q < s_0 < L - q$ (see Fig. 1 *c*).

If $\mathbf{V}(s_0, t)$ is the velocity of the cross-section s_0 then:

$$\begin{aligned}\mathbf{V}(s_0, t) = &-(1/C_T)\phi_T(s_0, t)\mathbf{T} \\ &- (1/C_N)\phi_N(s_0, t)\mathbf{N} - (1/C_B)\phi_B(s_0, t)\mathbf{B} \\ &+ \int_{|s-s_0|>q} \mathbf{U}_s(\mathbf{r}(s, t), \mathbf{r}(s_0, t), -\phi(s, t,)) \, ds \\ &+ \int_{0\le s\le L} \{\mathbf{V}_{si}(\mathbf{r}(s, t), \mathbf{r}(s_0, t), -\phi(s)) \\ &+ \mathbf{V}_{di}(\mathbf{r}(s, t), \mathbf{r}(s_0, t), -(a^2/4\mu)\phi(s, t))\} \, ds \\ &+ \mathbf{V}_{ext}(s_0, t) + O(\sqrt{\epsilon}), \qquad (3.3)\end{aligned}$$

where

$$C_T = \frac{8\pi\mu}{-2 + 4 \ln (2q/a)},$$

$$C_N = C_B = \frac{8\pi\mu}{1 + 2 \ln (2q/a)}. \qquad (3.4)$$

The term $\mathbf{V}_{ext}(s_0)$ represents the external flow field that is induced (at s_0) by sources other than moving segments of the cilium (neighboring cilia for example). It is assumed that $\mathbf{V}_{ext}(s_0)$ does not change significantly on the scale of a.

For simplicity, we refer to the group of the first three terms in (Eq. 3.3) as I, to the first integral as II and to the second integral as III.

Note that the minus signs on the right hand side of (Eq. 3.3) result from the fact that ϕ denotes the drag force exerted on the cilium. Hence, the intensity of the distribution of Stokelets along it is $-\phi$ (by force equilibrium).

Proof and remarks

The proof follows in a straightforward manner from Childress (1981) where he proved Lighthill's theorem. Let s_0 be a point on the center line of the cilium, and consider the segment $[s_0 - q, s_0 + q]$, as a straight cylinder (see Fig. 1 *c*). The parameter q is chosen as $q = a\epsilon^{(\theta-1)}$ for some $0 < \Theta < 1$. Calculate the velocity induced on the circumference of the cross-section s_0, by integrating over the interval $[s_0 - q, s_0 + q]$. Account only for the velocity that is induced by the Stokeslets and the Doublets which are distributed along the center line (with intensity as specified in the theorem and without the image system). The above choice of intensities (of Stokeslets and Doublets) yields, after some approximations, a constant velocity around the circumference of the cross-section s_0. We outline the procedure for the tangential component of the velocity:

Integrating the tangential velocity induced by the distribution of the Stokeslets (the Doublets do not have a tangential component) we obtain

$$-(1/8\pi\mu)\phi_T(s_0, t) \int_{-q}^{q} \phi_T(s, t)(1/r + s^2/r^3) \, ds, \quad (3.5)$$

where $r = (a^2 + s^2)^{1/2}$.

Approximating $\phi_T(s, t) \approx \phi_T(s_0, t)$ for s in $[-q, q]$, the expression in Eq. 3.5 becomes can be replaced by

$$-(1/8\pi\mu)\phi_T(s_0, t) \int_{-q}^{q} (1/r + s^2/r^3) \, ds + O(q). \quad (3.6)$$

After evaluating the above definite integral (with an error of $O((a/q)^2)$), expression 3.6 reduces to

$$-(1/C_T)\phi_T(s_0, t), \qquad (3.7)$$

where C_T was defined in Eq. 3.4.

A similar procedure, applied to the normal and binormal components, yields the rest of the terms in group I (see Childress [1981] for more detailed calculations). The deviation of the segment $[s_0 - q, s_0 + q]$ from the (ideal) straight cylindrical shape we assumed, restricts the curvature to be $O(q)$ so as not to change the order of magnitude of the error ($O(q)$). This concludes the effect of the local contributions (the "near field"). Next, we integrate the velocity induced by the singularities (including their image system) over the rest of the cilium (neglecting their variations around the circumference of the cross-section) and obtain the terms II (neglecting the Doublets) and III (which represents the contribution of the image system). One should note that the term III contains the effect of the image system of the singularities located along the segment $[s_0 - q, s_0 + q]$, which we did not account for in I. The errors introduced as a result of neglecting variations over the cross-section (in the "far field") are of order $O(a/q)$. An optimal value of q, in order to minimize the errors accumulated from the two specified sources, is $q = O(a/\sqrt{\epsilon})$ (i.e., $\Theta = \frac{1}{2}$), resulting in an error which is $O(\sqrt{\epsilon})$.

The external velocity, $\mathbf{V}_{ext}(s_0)$, is simply added. This is consistent if the error we add to our equation, as the result of neglecting variations over the circumference due to the external velocity, does not exceed $O(\sqrt{\epsilon})$ as well.

Some important points require further clarification. One is a comparison between our theorem and Lighthill's theorem (given in Eq. 3.2 above, for the case of an infinite cilium in infinite medium). In Lighthill's version, the only terms that are explicitly taken out of the integral sign, to (seemingly) form the local contributions to the velocity, are the normal and binormal ones. We denote the group of the first two terms of Eq. 3.2 by I′ and the integral by II′. The integral denoted by II′ can be divided into the sum of two integrals: the first one over the interval $\frac{1}{2}a\sqrt{e} < |s - s_0| < q$, and the second one over $|s - s_0| > q$. The first integral (after evaluating some definite integrals as in Childress [1981]), combined with I′ results in the term I appearing in Eq. 3.3. Hence, except for the image system (introduced in order to satisfy no-slip conditions on the substrate) and the

external flows (introduced in order to consider hydrodynamical interaction between cilia), the difference between our theorem and Lighthill's is only in the method of representation. The "advantage" of Lighthill's version is that the q-dependence is removed. However, this is exactly what makes his equation an integral equation of the first kind (with a singular kernel), and therefore a difficult one to solve. On the other hand, in our approach, we maintain a distance of at least q from the singularity located at s_0. Our equation is a well posed integral equation of the second kind, suitable for numerical solution. It follows from our proof that, provided $q = O(\sqrt{\epsilon})$, the solution is independent of q. This will be demonstrated numerically in Section 7. We refer here to Dresdner, Katz and Berger (1980) who developed a similar equation but without specifically bounding the resulting error. They also pointed out that one may be flexible in determining the distance from the singularity (i.e., q), although they did not give its optimal range.

To clarify the difference between our theorem and the G-H approach, Eq. 3.3 can be rearranged (see Eq. 3.9 below) to look like a G-H approximation plus some correcting terms (not necessarily small, as will be demonstrated). The G-H approximation can be derived using similar arguments to those we used in our theorem. The localization is achieved by considering only the near field contributions to the velocity. In order to "compensate" for neglecting the contributions of the far field, the value of q is taken to be much larger ($O(L)$) than specified in our theorem ($O(a/\sqrt{\epsilon})$). This is exactly where this approach fails to remain consistent. A flagellar or cilia segment of length $O(L)$ cannot be realistically considered as a straight cylinder. Therefore, although the expressions for the G-H drag coefficients are exactly the same as the coefficients in Eq. 3.4, their numerical value is different (due to the difference in the choice for the value of q). Specific choice of parameters, as presented in Section 6, will emphasize this difference.

It is also important to notice that equation 3.3, being suitable for modeling cilia in external flows, is applicable for multicilia problems. All one has to do is to calculate the induced external velocity, $\mathbf{V}_{ext}(s_0)$. This is done by integrating the distribution of Stokeslets (and possibly other singularities) over the neighboring cilia (i.e., every other cilium in the model). We only need to make certain that neglecting the variations of this velocity, over the scale of $O(a)$, does not introduce an error larger than $O(\sqrt{\epsilon})$. This is natural to assume for cilia configurations where the mean distances between them is of $O(\sqrt{\epsilon})$.

To present the relation (Eq. 3.3) as an integral equation for the drag force, define

$$\mathbf{G}(s_0, t) = \int_{|s-s_0|>q} \mathbf{U}_s(\mathbf{r}(s,t), \mathbf{r}(s_0,t), -\phi(s,t))\, ds + \int_{0\le s\le L} \{\mathbf{V}_{si}(\mathbf{r}(s,t), \mathbf{r}(s_0,t), -\phi(s)) + \mathbf{V}_{di}(\mathbf{r}(s,t), \mathbf{r}(s_0,t), -(a^2/4\mu)\phi(s,t))\}\, ds + \int_{\substack{0\le s\le L \\ \text{neighboring cilia}}} \mathbf{U}_s(\mathbf{r}(s,t), \mathbf{r}(s_0,t), -\phi(s,t))\, ds \quad (3.8)$$

and $g_N = C_N G_N$, $g_T = C_T G_T$, $g_B = C_B G_B$.
Here, $\mathbf{G}(s_0, t)$ represents the velocity induced at s_0 by the "far" segments, while $\mathbf{g}(s_0, t)$ represents the induced drag force per unit length.

The drag-velocity relation becomes:

$$\phi_N = -C_N V_N + g_N, \qquad \phi_T = -C_T V_T + g_T, \quad \phi_B = -C_B V_B + g_B. \quad (3.9)$$

As stated, Eq. 3.3 is valid only up to a distance q from each end of the cilium. Nevertheless, it was applied to the entire cilium. Such an approach has been justified by Barta and Liron (1988). Their research shows that $\phi(s)$ is small near the surface (to which the cilium is attached), due to the no-slip boundary conditions (because the local fluid velocities are very near zero). Consequently, the calculation errors we make near the surface are not crucial (of the order of a few percent).

Stated as it is, our theorem is applicable for modeling cilia attached to a surface and exposed to external flow. It could obviously be applied to simulate a single isolated flagellum (by dropping the image system and external flows).

Although Eq. 3.3 is valid for the general three-dimensional case, we restrict our simulations in this paper, to two-dimensional beats only, leaving the three-dimensional case to a subsequent report. In the two-dimensional model all cilia (modeled here by thin cylindrical filaments) are initially co-planar. Their excitation function is assumed to be two-dimensional and, consequently, so is their velocity. One can easily verify that, although the Stokeslets and the Doublets that appear in our equations are still three dimensional, under these specified restrictions, Eq. 3.3 has a zero binormal component. This implies that the cilia remain co-planar, which permits us to adapt two-dimensional equations of motion for the model.

4. EQUATIONS OF MOTION, INITIAL AND BOUNDARY CONDITIONS, SCALING

This section summarizes the equations of motion used in our simulations, and the process of choosing proper boundary and initial conditions.

(a) Equations

As explained, we restrict the motion to be two-dimensional. Since, except for the drag-velocity relation, the two-dimensional equations are similar to those used in H.-B. (Hines and Blum, 1978), the description will be brief. Introducing the variable $\alpha(s, t)$, defined in Section 2, we have $dx(s, t) = \cos(\alpha(s, t))ds$ and $dy(s, t) =$

$\sin(\alpha(s,t))ds$. Here, $x(s,t)$ and $y(s,t)$ are the coordinates of the center line of the cilium. The cilia in our model must maintain a constant length. Therefore, the above parameterization is advantageous since it automatically satisfies this inextensibility constraint (i.e., $(x_s)^2 + (y_s)^2 = 1$).

The force and moments balance yield

$$\phi_N = F_{Ns} + F_T\alpha_s, \tag{4.1}$$

$$\phi_T = F_{Ts} - F_N\alpha_s, \tag{4.2}$$

$$M_s = F_N, \tag{4.3}$$

while geometrical equations relate the components of the velocity

$$V_{Ns} = \alpha_t - V_T\alpha_s, \tag{4.4}$$

$$V_{Ts} = V_N\alpha_s \tag{4.5}$$

(recall that the subscripts s and t denote partial differentiation).

The above set of five equations together with Eq. 3.8 and the first two equations of 3.9 form a system of eight equations with nine unknowns. The missing equation to complete the system is the one that describes the internal mechanism of the cilium, which will substitute for the term $M_s\,(=F_N)$ in Eq. 4.3. In this paper F_N is modeled by

$$F_N = E_b\alpha_{ss} + S. \tag{4.6}$$

The first term of Eq. 4.6, being proportional to $k_s\,(=\alpha_{ss})$, is a passive term related to the stiffness of the cilium, and the parameter E_b is its bending resistance. The second term, S, is the active shear force generated inside the cilium. The choice for S is detailed in Section 5.

Eqs. 4.1–4.5 and 3.9 can be brought into a more convenient form. Differentiating Eqs. 4.2 and 4.3, using Eqs. 4.4, 4.5, and then 3.9, eliminates the velocity components and results in the following two equations:

$$F_{Nss} + (1 + C_{NT})F_{Ns}\alpha_s + F_T\alpha_{ss} = -C_N\alpha_t + C_{NT}F_N(\alpha_s)^2 + C_{NT}g_T\alpha_s + g_{Ns}, \tag{4.7}$$

$$F_{Tss} = (1 + C_{TN})F_{Ns}\alpha_s + C_{TN}F_T(\alpha_s)^2 + F_N\alpha_{ss} - C_{TN}g_N\alpha_s + g_{Ts}, \tag{4.8}$$

where $C_{TN} = C_T/C_N$ and $C_{NT} = C_N/C_T$.

From Eq. 4.8 it is clear that the tangential shear force is determined by the normal force and the shape of the cilium. This is the implicit outcome of the inextensibility constraint.

In order to make our equations nondimensional we introduce the normalized variables $s^* = s/L$, $t^* = wt$, $S^* = S/S_0$, where w is a typical frequency, L is the length of the cilium, and S_0 is a typical magnitude of shear force. In terms of these nondimensional variables, Eq. 4.7 changes to (after dropping the asterisks):

$$F_{Nss} + (1 + C_{NT})F_{Ns}\alpha_s + F_T\alpha_{ss} = -(C_N wL^2/S_0)\alpha_t + C_{NT}F_N(\alpha_s)^2 + C_{NT}g_T\alpha_s + g_{Ns}. \tag{4.9}$$

Eq. 4.8 becomes

$$F_N = E_b/(S_0L^2)\alpha_{ss} + S. \tag{4.10}$$

Two dimensionless parameters, $C_N wL^2/S_0$ and $E_b/(S_0L^2)$, appear in our model. $E_b/(S_0L^2)$ measures the relative importance of the elastic resistance of the cilium compared with the actively generated shear force, while $C_N wL^2/S_0$ measures the balance between typical magnitudes of the hydrodynamic drag force and active shear force.

From here on all the variables are in nondimensional form. For convenience, we omit the asterisks. The specific choices for w, L, S_0 will be discussed in Section 6.

(b) Boundary and initial conditions

Since our equations do not determine the orientation of the cilium at the anchor we must choose constitutive equations. The conditions

$$\alpha(0,t) = \pi/2, \tag{4.11}$$

$$\alpha_s(0,t) = 0, \tag{4.12}$$

keep the cilium erect at the anchor. Since the distal end is free, all shear forces and moments must vanish there, and hence

$$F_N(1,t) = F_T(1,t) = 0. \tag{4.13}$$

(Note that, in the nondimensional notation, $s = 1$ at the distal end.)

Eq. 4.1, 4.2, 4.12, and the fact that there is no drag at the anchor yield

$$F_{Ts}(0,t) = F_{Ns}(0,t) = 0. \tag{4.14}$$

Next, using (4.10) up to the distal end we obtain

$$\alpha_{ss}(1,t) = -S(1,t). \tag{4.15}$$

To complete the boundary conditions we chose

$$\alpha_s(1,t) = 0, \tag{4.16}$$

which implies that the distal end of the cilium is straight. Note that integrating Eq. 4.3 yields

$$M(0,t) = -\int_0^1 F_N(s,t)\,ds, \tag{4.17}$$

which means that the total active shear is balanced by the moment generated at the anchor.

As for initial conditions, unless otherwise specified, we used:

$$\alpha(s,0) = \pi/2, \tag{4.18}$$

which means that the cilium stands erect at time $t = 0$.

5. MODELING THE INTERNAL MECHANISM OF THE CILIA

We describe here the detailed modeling of the internal mechanism of the cilium, which we call the "engine." F_T and F_N are the components of the forces developed inside the cilium by the internal filaments. Since F_T is determined by F_N (Eq. 4.8), an equation for F_N is to be provided. It is clear that simulations with various engines are possible, by choosing different expressions for F_N. Consequently, all previous models of internal mechanisms (Brokaw, 1970; Rikmenspoel, 1971, 1973, 1976, 1982; Hines and Blum, 1978, 1979*a*; and others) may be incorporated into our approach.

As the main goals in this research were to simulate single cilium and multicilia configurations using an accurate and consistent model, rather than to test specific mechanisms, general basic concepts were used in the construction of our engine. These proved to be good enough to model ciliary propulsion. The beat patterns achieved by this model show resemblance to some experimentally observed beats (Sleigh, 1960; Machemer, 1972) and to other simulated ciliary motion (Rikmenspoel, 1971, 1973, 1976, 1982).

The engine we modeled here is load dependent. This means that the normal shear force, F_N, is not completely predetermined, but rather depends on the instantaneous shape of the cilium (thus implicitly on the external forces acting on it). This can be achieved by introducing a term that depends on the changes in shape (i.e., the curvature gradient) of the cilium. Consequently, we assumed (in accordance with other acceptable models (Lubliner, 1973; Rikmenspoel, 1971, 1973, 1976, 1982; Hines and Blum, 1978, 1979*a*)) that the engine consists of two contributions as in Eq. 4.6. The first term of Eq. 4.6 represents the internal elasticity (which is implicitly the load dependence) and the second one represents the active shear generated by the sliding filaments.

For the active shear, S, in Eq. 4.6 we chose

$$S(s, t) = f(s)R(wt). \tag{5.2}$$

$R(wt)$ is a periodic function where w is the frequency of the engine. The term $f(s)$ determines the amplitude of the motion. If $R(wt)$ is chosen to be nonsymmetrical during a beat cycle, the resulting motion has two distinct phases, and, combined with an appropriate choice of $f(s)$, could simulate the recovery and effective strokes observed experimentally.

In all simulations we refer to two kinds of engines: the symmetrical engine (i.e., no difference between the recovery and effective strokes) and the nonsymmetrical engine.

We used

$$S(s, t) = (\pi/2)C_N w(L^2/S_0)(s^2 - 1) \times \sin(2\pi t)\cdot c_1(t)\cdot c_2(s, t), \tag{5.3}$$

where $c_1(t)$ is responsible for creating two distinct phases. It is defined periodically over the (dimensionless) beat cycle.

$$c_1(t) = \begin{cases} a_1 & 0 \le t \le t_1 \\ a_2 & t_1 < t \le 1. \end{cases} \tag{5.4}$$

Here t_1 is the duration of the "effective stroke" and a_1, a_2 are amplitude coefficients.

The parameter $c_2(s, t)$ divides the cilium into two portions: active and nonactive (with length a_3). It receives different values during the effective and recovery strokes.

$$c_2(s, t) = \begin{cases} 1 & 0 \le s \le 1, \quad 0 \le t \le t_1 \\ 1 & 0 \le s \le a_3, \quad t_1 \le t \le 1 \\ 0 & a_3 < s \le 1, \quad t_1 \le t \le 1. \end{cases} \tag{5.5}$$

Note that for $a_1 = a_2$ (and $c_2 \equiv 1$) the engine is symmetrical.

6. NUMERICAL PROCEDURES AND PARAMETERS CHOICE

We now describe the numerical methods used to obtain solutions, and the parameters we used.

Starting at a certain time t and cilium shape $\alpha(s, t)$ one can calculate F_N by using Eq. 4.10 and 5.3–5.5. Next, using Eq. 4.9, F_T is calculated (computing g_T and g_N iteratively, starting with their values at the previous time step).

The values of ϕ_N and ϕ_T are then obtained from Eqs. 4.1 and 4.2. Now, Eq. 3.8 is used to calculate a new estimate for g_T and g_N. Two coordinate systems must be used simultaneously: local (T, N), and global (x, y). The reason is that Eq. 3.8 depends on the global location of the singularities along the cilia (due to the no-slip condition at $y = 0$).

The whole procedure described above is repeated several times to achieve convergence. It was found that after five iterations no further changes (in the calculated variables) were detected up to the fourth significant digit.

With the current values, we use Eq. 4.9 to propagate $\alpha(s, t)$ in time. Since Eq. 4.9 is nonlinear, an iterative solution method was applied.

A more detailed description of a similar numerical problem can be found in H.-B. We emphasize the main differences. In our equations we also have the terms g_T and g_N, and therefore we include their (iterative) calculation into the process. Secondly, in the numerical solution we used the Crank-Nicholson method (which is unconditionally stable) to avoid instability. This method is accurate to the order of ds^2 and dt^2 (where ds and dt are the spatial and time steps, respectively). The method described in H.-B. was a variation on the fully implicit

method, which is exact to the order of ds^2 and dt only (in a later reference [Hines and Blum, 1979] this method of solution is indeed implicitly referred to as a "fully implicit scheme"). Applying the Crank-Nicholson method does not add any significant computational effort so it is preferable in this case.

After initializing the motion of the cilia, some time elapses before they reach their periodic beat cycle. In order to ensure that what we observed was indeed the final periodic beat, the following technique was used: recording the positions of the cilia during the beat cycles, we saved two cycles backwards. Then, comparing the current beat pattern to the previous one, we could decide if the two beat patterns were already "identical." We found that six cycles were enough to obtain the desired periodic beat. Throughout all the simulations we used 31 discretization points along each of the cilia, for the purpose of calculation. It was verified that no additional changes occurred as a result of increasing this number of points.

The parameters we used in our simulations are:

$L = 10\ \mu m$, $a = 0.1\ \mu m$:	chosen to match typical cilia dimensions;
$q = 1\ \mu m$:	to meet the demand $q = O(a/\sqrt{\epsilon})$.
$S_0 = 10^{-12}$ Newtons:	a typical shear force magnitude, see [H.-B.];
$E_b = 25 \cdot 10^{-24}$ Newtons m^2:	as in H.-B.;
$w = 25\ rad \cdot s^{-1}$:	a typical beat frequency.

With these constants, the scaling as in Section 4, and Eq. 3.4 the dimensionless values of μ (the viscosity of water), C_T, C_N are:

$$\mu = 2.5, \quad C_T = 6.293, \quad C_N = 8.898.$$

Note that our resistance coefficients are different from the G-H "classical" values: $C_N = 12.5$ and $C_T = (1/2)C_N$ for cilia in water (as H.-B., but in dimensionless form).

In modeling the engine, the following parameters were used for the nonsymmetrical engine:

$$a_1 = 2, \quad a_2 = 5, \quad a_3 = 0.4, \quad t_1 = 0.35,$$

and the following parameters for a symmetrical engine:

$$a_1 = 2, \quad a_2 = 2, \quad a_3 = 1, \quad t_1 = 1.$$

The spatial and time steps for the numerical schemes were:

$dt = 0.02$:	i.e., 50 time steps per one beat cycle (decreasing the time step left the results unchanged);
$ds = 1/30$:	i.e., 31 discretization points on each cilium.

7. RESULTS

This section summarizes the results of the simulations and briefly describes the animated-displaying techniques we suggest for such cases.

Results for a single cilium

Fig. 2 presents the beat cycle of a cilium having (*a*) a nonsymmetrical (two stroke) engine, and (*b*) a cilium with a symmetrical engine. The snapshots were taken at (dimensionless) time intervals of 0.1 (i.e., 10 snapshots per cycle). As can be seen, choosing parameters as specified in Section 6, we obtained beat patterns that emulated the two distinct phases of the cycle, namely: the effective stroke (in which the cilium is almost straight) and the recovery stroke (in which the cilium is bent and is subjected to less hydrodynamic resistance, because a greater proportion of its motion is tangential to its own centerline). Varying $c_2(s, t)$ and $c_1(t)$ gave different beats, some of which involve much larger tangential deviation from the erect position, at the end of the effective stroke. This demonstrates the fact that our model is capable of creating a variety of beat patterns (depending on

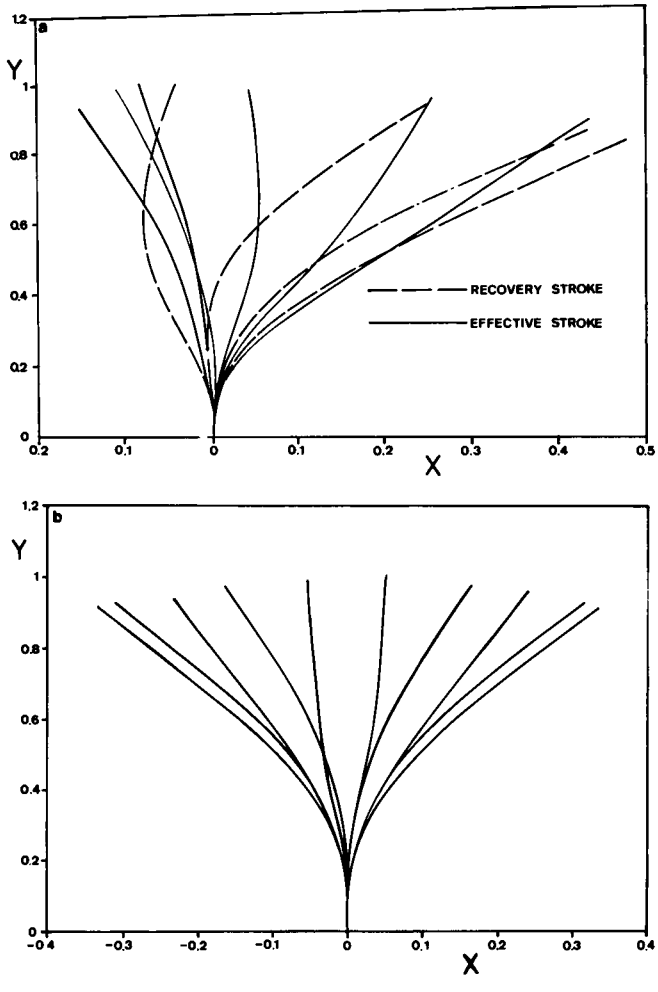

FIGURE 2 Snapshots of a beat cycle of a single cilium (10 snapshots per one beat cycle, i.e., dimensionless time intervals of 0.1). (*a*) Nonsymmetrical engine. The effective and recovery strokes are plotted differently to distinguish between them. The engine parameters used in this simulation are $a_1 = 2$, $a_2 = 5$, $a_3 = 0.4$, $t_1 = 0.35$ (see Eqs. 5.3–5.5). (*b*) Symmetrical engine. The engine parameters used in this simulation are $a_1 = 2$, $a_2 = 2$, $a_3 = 0.4$, $t_1 = 0.35$ (see Eqs. 5.3–5.5).

the engine parameters used). The beat produced by these models resemble experimentally observed beats (Sleigh, 1960; Machemer, 1972) and other simulated ciliary motions (Rikmenspoel, 1971, 1973, 1976, 1982).

In order to demonstrate the advantage of Eq. 3.3 (or 3.9) over the G-H approach and over Lighthill's equation we draw attention to the following results, obtained by simulating the motion of a single cilium with a nonsymmetrical engine.

(*a*) Different choices of the parameter q (in the range of $O(a/\sqrt{\epsilon})$) do not change the resulting solution, which is consistent with the theoretical results as stated in the Theorem in Section 3. This was verified by altering q/L within a range of 0.07 to 0.17 (for $\epsilon = 0.01$), and measuring the maximal distance between the locations of matching points along the centerlines, in the different beat cycles (divided by the total length of the cilium). These changes caused relative deviations of less than 0.5% in the beat cycles, compared with the results for $q/L = 0.1$.

(*b*) The velocity field G (induced by the far field singularities, (see Eqs. 3.8 and 3.9), is not always small compared with I, the parallel expression to the G-H resistance coefficients (see Eqs. 3.3–3.4) (the local force-velocity relation), comparing the tangential and normal components, respectively. Neither is it constant (or close to being constant). The term G could be interpreted as a "correction term" that must be added in order to correct the G-H approximation (note that the terms g_N and g_T stand for all of the contributions other than the local ones). Our results, therefore, show that the G-H approach (and other resistive force theories) is not an accurate approximation for our problem since no localization is possible (at least when a surface is present). This point is made clear in Fig. 3, where the ratios $|g_T/\phi_T|$ and $|g_N/\phi_N|$ (measuring the relative size of the drag due to the nonlocal correction term, compared with the local drag force) are plotted as a function of the location along the cilium. The local spike at $s = 0.9$ is the result of ϕ_N passing through zero. This does not upset the simulations since the model never sees the local drag force as the denominator of a fraction.

(*c*) From Fig. 3 we see that $|g_T/\phi_T|, |g_N/\phi_N| < 1$. This is the case in general, and shows that Eq. 3.9 is "diagonally dominant". By diagonally dominant we imply that (after proper discretization) solving Eq. 3.9 for ϕ becomes equivalent to solving a linear system of equations (for each component), possessing a diagonally dominant coefficients matrix. It implies that an iterative solution strategy converges.

(*d*) $|(1/C_T)\phi_T|$, the local contribution to the tangential velocity is not necessarily small compared with $|(1/C_N)\phi_N|$, the local contribution to the normal velocity (see Eq. 3.9), as is clearly shown in Fig. 4. This implies that had we used Lighthill's equation (3.2) to solve numerically for ϕ, the matrix of coefficients would not be diagonally dominant. This would imply severe numerical difficulties. For comparison purposes we nevertheless obtained the numerical solution of the cilium equations using Lighthill's approach. As expected, it required a significantly finer grid (150 points on the cilium as opposed to 31 with our method), more iterations for convergence at each time step, and smaller time steps (one-twentieth of the time step used with our method). This confirms that Lighthill's equation is less appropriate for such simulations, especially when several cilia are treated (the computational complexity is proportional to the square of the total number of points over all of the cilia).

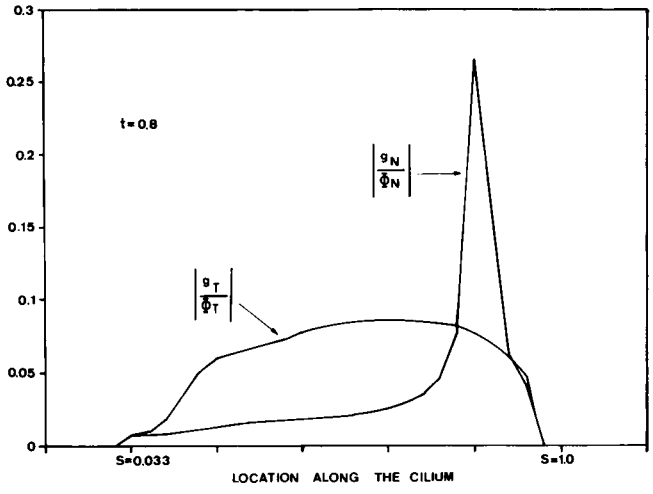

FIGURE 3 Comparing the tangential and the normal drag force, induced by far segments of the cilium, to the local drag force (the ratios $|g_T/\phi_T|$ and $|g_N/\phi_N|$, respectively) (see Eq. 3.9) at one time step ($t = 0.8$) during the recovery stroke, as a function of location along the cilium. The engine used in this case is a nonsymmetrical engine as described in Section 4. The engine parameters used in this simulation are $a_1 = 2$, $a_2 = 5$, $a_3 = 0.4$, $t_1 = 0.35$ (see Section 5).

(*e*) Applying the G-H approximation (following H.-B. we used the corrected coefficients, suitable for flagella in water, suggested by Brokaw [1970]) to simulate the same cilium, introduced a deviation of more than 15% in the beat pattern, compared with the results we obtained using our theorem. The comparison is done by measuring the maximal deviations of the final beat pattern, obtained by our approach, from the final beat pattern obtained by using the G-H method. This exemplifies the inaccuracy involved in the use of the G-H approach.

Results for multicilia configurations

Multicilia configurations were also successfully modeled. Such configurations consist of a row of beating cilia where their interaction is taken into account. We were able to check the influence range of the cilia on each other (i.e., the maximal spacing between cilia, for which the interaction could still be distinguished). This was obtained by a trial-and-error process. Our conclusion is that this influence range is $\sim$1.2 (cilium lengths).

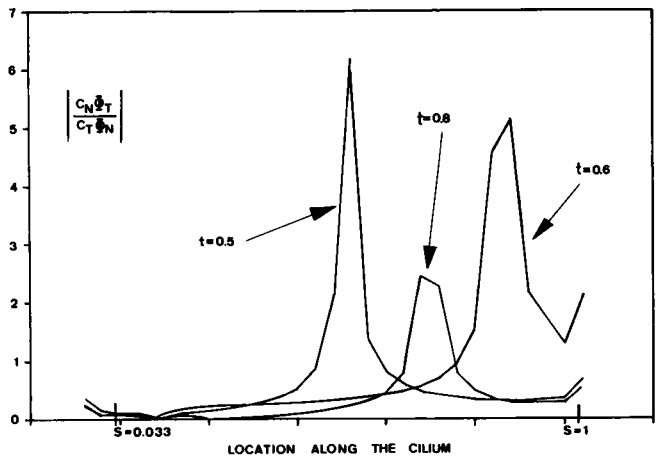

FIGURE 4 Comparing between the local contribution to the tangential velocity and the local contribution to the normal velocity (the ratio $|C_N \cdot \phi_T / C_T \cdot \phi_N|$) (see Eq. 3.9) at three time steps ($t = 0.5, t = 0.6, t = 0.8$) during the recovery stroke, as a function of the location along the cilium. The engine used in this case is a nonsymmetrical engine as described in Section 4. The engine parameters used in this simulation are $a_1 = 2$, $a_2 = 5$, $a_3 = 0.4$, $t_1 = 0.35$, see Section 5.

Beyond a distance of 0.8 though, a sharp drop of the influence intensity was detected. This range is larger than what was estimated in other researches (Sleigh, 1984).

In all of the following configurations the (dimensionless) chosen ciliary spacing was 0.2, in accord with the typical spacing, observed in ciliates such as Opalina and Paramecium (Machemer, 1972).

Fig. 5 demonstrates the fact that the interaction between cilia changes the original beat patterns. A row of five cilia having a symmetrical engine (compare with Fig. 2) was examined. Fig. 5 *a* shows snapshots of the five cilia (with spacing of 0.3) at a two different time steps. Fig. 5 *b* shows the entire beat cycle of cilia number 1, 3, and 5. The beat patterns changed and became nonsymmetrical. In fact, one could observe that only the middle cilium maintained a symmetrical beat (though different from the original one). Another phenomenon was observed by comparing the beat cycles of cilia number 1 and 5 (or 2 and 4). Their beats are the mirror image of each other. This is predictable, since the Stokelets kernels possess a mirror image symmetry themselves (i.e., the velocity $\mathbf{U}_s(\mathbf{r}, \mathbf{r}_0, \phi)$ is the mirror image of $\mathbf{U}_s(\mathbf{r}_0, \mathbf{r}, \phi)$). The same phenomenon occurred in all multicilia configurations having symmetrical engines. Whenever the number of cilia was even, the mirror-image symmetry was complete. Whenever it was odd, all cilia, except for the middle one (that had itself a symmetrical beat pattern), kept the mirror-image symmetry.

Finally we show the effect of changing the viscosity as demonstrated in Fig. 6, *a* and *b*. Modeling the same five cilia configuration we increased the viscosity to five times that of water. As reported in some experiments (Sleigh, 1960), it produced different beat patterns than in experiments using water. Fig. 6, *a* and *b*, are to be compared with the analogous Fig. 5, *a* and *b*, respectively.

We conclude with the displaying technique we designed for the problem. We found that the ciliary beats, and especially the metachronal coordination, could not be presented convincingly in drawing. Even if we had sufficient space to print all the snapshots of the beat cycles successively, it would not be effective. Accordingly, we wrote a computer animation program for this purpose. In animated sequences, the beats and metachronism are easy to observe and compare. Our animating program has slow and fast motion control, forwards and backwards play, and frame-by-frame (forwards and backwards) advance. All the relevant results reported in the paper (and some additional ones), are presented in this way, and the resulting demonstration program is available upon request.

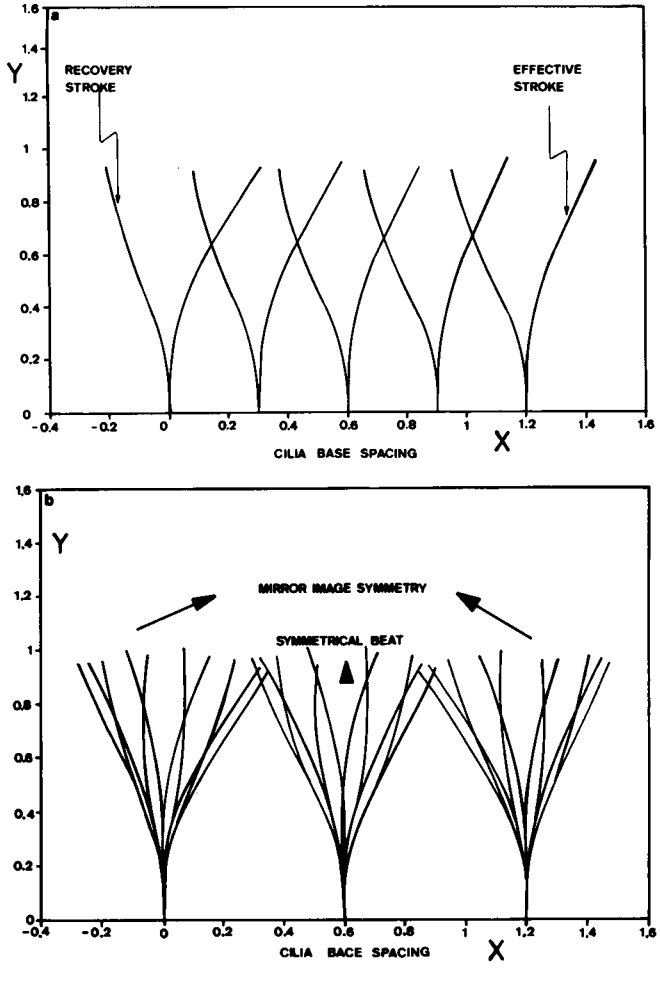

FIGURE 5 A configuration of five cilia in a row, with a symmetrical engine (ciliary spacing, 0.2). (*a*) Two snapshots: one during the effective stroke ($t = 0.2$), and the other during the recovery stroke ($t = 0.6$). (*b*) The entire beat cycle (10 snapshots) of cilia number 1, 3, and 5. The engine parameters used in this simulation are $a_1 = 2$, $a_2 = 2$, $a_3 = 0.4$, $t_1 = 0.35$ (see Eq. 5.3–5.5).

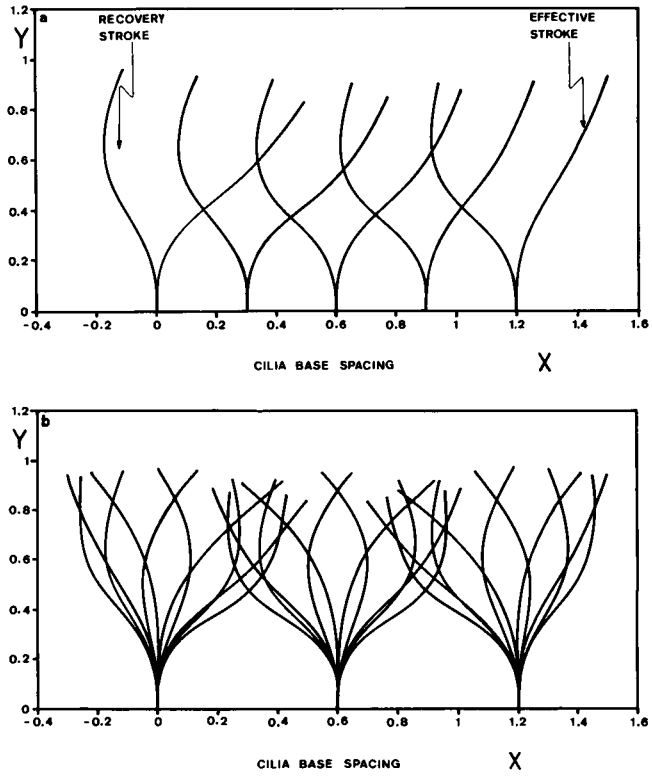

FIGURE 6 A Snapshot of five cilia (ciliary spacing 0.2) in a row with a symmetrical engine (to be compared with Fig. 5). The viscosity here is five times that of water. The periodic beat pattern is shown at two snapshots taken (*a*) during the effective stroke ($t = 0.2$) and (*b*) during the recovery stroke ($t = 0.6$). The engine parameters used in this simulation are the same as in Fig. 5.

8. DISCUSSION

Our results demonstrate the advantage of applying our approach to model ciliary beating. The new drag-velocity equation avoids the inconsistencies and the limitations of the G-H approximation. It also overcomes the difficulties emerging from Lighthill's equation. This leads to a rigorous model that produces similar beats to those observed experimentally.

The suggested model is flexible and can yield a variety of beat patterns, according to the parameters applied to the engine equation. It can be applied to simulate internal mechanisms other than those described in the paper. Even so, not every engine is suitable to reproduce ciliary beats. Different models for the internal mechanism, governing the motion of cilia and flagella, exist in the literature. They all consist of two contributions: passive bending resistance, modeling the stiffness of the cilium (flagellum), and active shear, generated by its sliding filaments. The passive contribution is identical in most of the models, whereas differences appear in the way the active shear is modelled. Brokaw, in his successive series of papers (1970, 1972a, 1972b, 1975, 1976), suggested an active mechanism controled by the local curvature gradient, with some time delay, forming a difference equation. A different version has been suggested by H.-B. (1978, 1979a). They replaced Brokaw's shear force equation with a differential equation. This eliminates the need for the time delay, reduces the computational effort involved in solving the resulting system of equations, and improves the stability of the numerical schemes. The above engines were used to simulate the motion of a single flagellum (usually longer and thus more slender than a cilium) free at both ends. When ciliary boundary conditions were applied to these internal mechanisms, they did not produce ciliary beat patterns. Evidently, this is because these engines are designed to produce travelling waves along the flagellum, rather than to simulate the effective and recovery strokes of a cilium. Indeed Hines and Blum (1979*b*) reported on the following numerical experiments: for a short cilium, no motion occurred at all. For a longer one, the resulting motion resembled that of a flagellum. Their conclusion was that using an engine suitable for producing flagellar motion, with ciliary boundary conditions, is inadequate for modelling ciliary propulsion. Engines that produced ciliary beat patterns were suggested by Rikmenspoel (1973, 1976, 1982). Consequently, we constructed our engine in a similar manner.

The two-dimensional beat patterns obtained by our model can be changed by choosing different engine parameters. Since we simulated two-dimensional beats, we were forced to restrict the amplitude of the beats in order to avoid cilia colliding into each other while beating. This becomes especially important when the cilia are not started simultaneously (however, results concerning these cases were not reported in this paper). Indeed it is hard to imagine beats with large amplitude and phase lags between the beats unless the recovery stroke is not in the plane of the effective stroke.

In light of the computational complexity involved with our suggested method, compared with that of the G-H approach, it is natural to wonder whether the latter would still be preferable, despite its inconsistencies for an isolated cilium. A partial answer may be found in the work of Johnson and Brokaw (1979) who tried to correct the G-H approximation. They suggested that an empirical increase of the G-H drag coefficients improved the results, for the case of a flagellum free at both ends. No such adjustment was found for a flagellum having a cell body attached to it. Problems dealing with flagella with a (spherical) cell body demand somewhat finer analysis and suitable methods have been accordingly developed for these cases (see Section 3). Similarly, the presence of surfaces, from which cilia emerge, yields nonlocal (significant) effects (see also Barta and Liron, 1988). Since any reliable model for ciliary propulsion must consider such a surface, it is clear that applying RFT to these cases is inadequate. Comparing the results obtained by using our theorem to those obtained from the G-H approximation supports this assertion.

Multicilia configurations were investigated in this paper, for the first time, as a dynamical process, taking the hydrodynamical interaction into account. We showed that beat patterns change as a result of the presence of neighboring cilia. This fact is an important observation since in most experiments the cilia are not isolated, hence the observed beats are already the overall result of the cilia interactions. The effect of increased viscosity for multicilia configurations has also been modeled. Looking at Fig. 6, *a* and *b*, it might seem that the cilia gained wider amplitudes with increased viscosity but it should rather be regarded as a change in the beat pattern. In this example the engine is designed to generate back and forth motions while the cilium is basically straight. Due to the increased viscosity the engine encounters higher resistance and yields. Therefore, the cilium becomes curved and since it is inextensible this means that is does not extend as high as before the viscosity increase. The result is beat patterns where the cilium is bent, beats lower, and thus reaches sideways further.

Our approach presents a general reliable modeling tool for investigating the metachronism phenomenon. We have already used it to obtain some preliminary results concerning the formation of metachronism, which support the conjecture that it is a hydrodynamical effect. These results will be presented in a following report.

Simulations with a larger (than twenty) number of cilia have not been performed, because of the lengthy computational time. One should note that it is a only a technical limitation. All simulations reported here were done on an IBM PS/70 computer. However, due to the reported limited influence range of cilia (on their neighbors), and to typical dimensions of relevant configurations, an array of twenty cilia is sufficiently large to draw conclusions from.

APPENDIX

Singular solutions of the Stokes equations

The singular solutions of the Stokes equations, used in the theorem in Section 3, are presented in Eqs. A.1–A.4. The definitions are as in the theorem.

Let

$\mathbf{d} = \mathbf{r} - \mathbf{r}_0$,

$\mathbf{R}_0 = (r_{01}, r_{02}, -r_{03})$ (the image of $\mathbf{r}_0$ with respect to $x_3 = 0$),

$\mathbf{D} = \mathbf{r} - \mathbf{R}_0$,

$h = |r_{03}|$, the x_3 component of $\mathbf{r}_0$,

$d = |\mathbf{d}|$, $D = |\mathbf{D}|$,

$\mathbf{x}_3$ = unit vector in the x_3 direction.

Then

$$(8\pi\mu)\mathbf{U}_s(\mathbf{r}, \mathbf{r}_0, \phi) = \frac{\phi}{d} + \frac{(\phi\cdot\mathbf{d})\mathbf{d}}{d^3}, \tag{A.1}$$

$$(8\pi\mu)\mathbf{U}_d(\mathbf{r}, \mathbf{r}_0, \phi) = \frac{\phi}{d^3} - \frac{3(\phi\cdot\mathbf{d})\mathbf{d}}{d^5}, \tag{A.2}$$

$$\begin{aligned}(8\pi\mu)&\mathbf{U}_{si}(\mathbf{r}, \mathbf{r}_0, \phi)\\ &= \mathbf{U}_s(\mathbf{r}, \mathbf{r}_0, \phi) - \frac{\phi}{D} - \frac{(\phi\cdot\mathbf{D})\mathbf{D}}{D^3} + 2h\left\{\frac{3(\phi\cdot\mathbf{D})x_3\mathbf{D}}{D^5}\right.\\ &\quad - \frac{6(\phi\cdot\mathbf{x}_3)(\mathbf{D}\cdot\mathbf{x}_3)x_3\mathbf{D}}{D^5} + \frac{(\phi\cdot\mathbf{D})\mathbf{x}_3}{D^3} + \frac{(\phi\cdot\mathbf{x}_3)\mathbf{D}}{D^3}\\ &\quad \left. - \frac{2h(\phi\cdot\mathbf{x}_3)\mathbf{x}_3}{D^3} - \frac{\mathbf{x}_3\phi}{D^3}\right\},\end{aligned} \tag{A.3}$$

$$\begin{aligned}(8\pi\mu)&\mathbf{U}_{di}(\mathbf{r}, \mathbf{r}_0, \phi)\\ &= \mathbf{U}_d(\mathbf{r}, \mathbf{r}_0, \phi) - \frac{\phi}{D^3} + \frac{3(\phi\cdot\mathbf{D})\mathbf{D}}{D^5}\\ &\quad - \frac{6(\phi\cdot\mathbf{x}_3)(2x_3 + h)\mathbf{D}}{D^5} - \frac{6(\phi\cdot\mathbf{D})h\mathbf{x}_3}{D^5}\\ &\quad + \frac{12(\phi\cdot\mathbf{x}_3)(\mathbf{D}\cdot\mathbf{x}_3)(h - x_3)\mathbf{x}_3}{D^5}\\ &\quad - \frac{30\,x_3(\phi\cdot\mathbf{x}_3)(\phi\cdot\mathbf{D})\mathbf{D}}{D^7} + \frac{60(\phi\cdot\mathbf{x}_3)x_3(\mathbf{D}\cdot\mathbf{x}_3)^2\mathbf{D}}{D^7}\\ &\quad + \frac{6(\mathbf{D}\cdot\mathbf{x}_3)x_3\phi}{D^5}.\end{aligned} \tag{A.4}$$

We would like to thank an anonymous referee for his careful reading of an earlier version of this paper, and his suggestions, which greatly improved the presentation of the results.

The research was supported by the Fund for Promotion of Research at the Technion, Israel Institute of Technology, and by a grant from the Basic Research Foundation, The Israel Academy of Sciences and Humanities.

Received for publication 17 December 1990 and in final form 14 April 1992.

REFERENCES

Barta, E., and N. Liron. 1988. Slender body interactions for low Reynolds numbers, part I: body-wall interactions. *SIAM. J. Appl. Math.* 48:993–1008.

Blake, J. R. 1972. A spherical envelope approach to ciliary propulsion. *J. Fluid Mech.* 46:199–208.

Brennen, C., and H. Winet. 1977. Fluid mechanics of propulsion by cilia and flagella. *Annu. Rev. Fluid. Mech.* 9:339–398.

Brokaw, C. J. 1970. Bending moments in free-swimming flagella. *J. Exp. Biol.* 53:445–464.

Brokaw, C. J. 1972a. Computer simulation of flagellar movement. I. Demonstration of stable bend propagation and bend initiation by the sliding filament model. *Biophys. J.* 12:564–586.

Brokaw, C. J. 1972b. Computer simulation of flagellar movement. II. Influence of external viscosity on movement of the sliding filament model. *J. Mechanochem. Cell Motil.* 1:203.

Brokaw, C. J. 1975. Cross bridge behavior in a sliding filament model for flagella. *In* Molecules and Cell Movement. S. Inoue, and R. E. Stephens, editors. Raven Press, New York. 165–179.

Brokaw, C. J. 1976. Computer simulation of flagellar movement. IV. Properties of an oscillatory two-state cross-bridge model. *Biophys. J.* 16:1029–1041.

Brokaw, C. J., and D. Rintala. 1975. Computer simulation of flagellar movement. Models incorporating cross-bridge kinetics. *J. Mechanochem. Cell Motil.* 3:77–86.

Brokaw, C. J., and D. Rintala. 1977. Computer simulations of flagellar

movement. V. Oscillation of cross-bridge models with an ATP-concentration-dependent rate function. *J. Mechanochem Cell Motil.* 4:205–227.

Childress, S. 1981. Mechanics of Swimming and Flying. Cambridge University Press, New York. 51–60.

Dresdner, R. D., D. F. Katz, and S. A. Berger. 1980. The propulsion by large amplitude waves of uniflagellar micro-organism of finite length. *J. Fluid. Mech.* 97:591–621.

Gray, J., and G. Hancock. 1955. The propulsion of sea-urchin spermatozoa. *J. Exp. Biol.* 32:802–814.

Higdon, J. J. L. 1979a. A hydrodynamic analysis of flagellar propulsion. *J. Fluid. Mech.* 90:685–711.

Higdon, J. J. L. 1979b. The hydrodynamics of flagellar propulsion: helical waves. *J. Fluid. Mech.* 94:331–351.

Higdon, J. J. L. 1979c. The generation of feeding currents by flagellar motion. *J. Fluid. Mech.* 94:305–330.

Hines, M., and J. J. Blum. 1978. Bend Propagation in Flagella. I. Derivation of equations of motion and their simulation. *Biophys. J.* 23:267–340.

Hines, M., and J. J. Blum. 1979a. Bend propagation in flagella. II. Incorporating of dyenin cross-bridge kinetics into the equations of motion. *Biophys. J.* 25:421–442.

Hines, M., and J. J. Blum. 1979b. Biophysics of flagellar motility. *Rev. Biophys. Quart.* 12:103–180.

Johnson, R. E., and C. J. Brokaw. 1979. Flagellar hydrodynamics: a comparison between resistive-force theory and slender-body theory. *Biophys. J.* 25:113–127.

Lighthill, J. L. 1975. *Mathematical Biofluiddynamics.* Regional Conference Series in Applied Mathematics. SIAM. Philadelphia. 45–62.

Lighthill, J. L. 1976. Flagellar hydrodynamics. *SIAM Rev.* 18:161–230.

Liron, N. 1978. Fluid transport by cilia between parallel plates. *J. Fluid Mech.* 86:705–726.

Liron, N. 1984. Stokeslets arrays in a pipe and their application to ciliary transport. *J. Fluid Mech.* 143:173–195.

Liron, N., and S. Mochon. 1976. The discrete-cilia approach for propulsion of ciliated microorganisms. *J. Fluid Mech.* 75:593–607.

Lubliner, J. 1973. An analysis of interfilaments shear in flagella. *J. Theor. Biol.* 31:1–23.

Machemer, H. 1972. Ciliary activity and metachronism in protozoa. *In* Cilia and Flagella. M. A. Sleigh, editor. Academic Press, Inc., New York. 199–286.

Myerscough, M. R., and M. A. Swan. 1989. A model for swimming unipolar spirilla. *J. Theor. Biol.* 139:201–218.

Phan-Thien, N., T. Tran-Cong, and M. Ramia. 1987. A boundary-element analysis of flagellar propulsion. *J. Fluid. Mech.* 185:533–549.

Ramia, M. 1991. Numerical methods for the locomotion of spirilla. *Biophys. J.* 60:1057–1078.

Rikmenspoel, R. 1971. Contractile mechanisms in flagella. *Biophys. J.* 11:446–463.

Rikmenspoel, R. 1973. The contractile mechanism in cilia. *Biophys. J.* 13:955–993.

Rikmenspoel, R. 1976. Contractile events in the cilia of Paramecium, Opalina Mytilus and Phragmatopma. *Biophys. J.* 16:445–470.

Rikmenspoel, R. 1982. Ciliary contractile model applied to flagellar motion. *J. Theor. Biol.* 96:617–645.

Sleigh, M. A. 1960. The form of beat in cilia of Stentor and Opalina. *J. Exp. Biol.* 37:1–33.

Sleigh, M. A. 1962. The Biology of Cilia and Flagella. Pergamon Press, Oxford.

Sleigh, M. A. 1984. The integrated activity of cilia: function and coordination. *J. Protozol.* 31 (1):16–21.

Sleigh, M. A., J. R. Blake, and N. Liron. 1988. The propulsion of mucus by cilia. *Am. Rev. Respir. Dis.* 137:726–741.